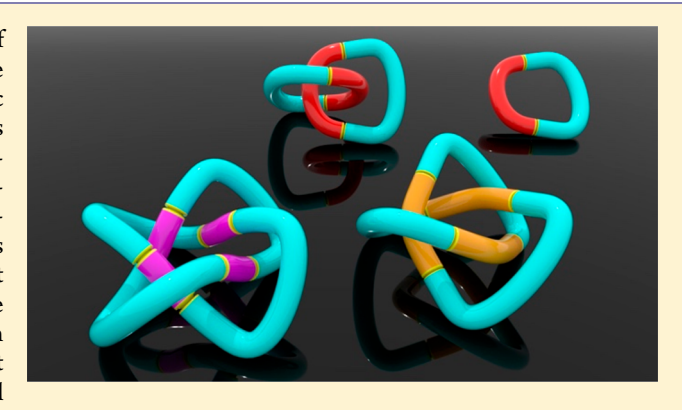


A Strategy to Synthesize Molecular Knots and Links Using the **Hydrophobic Effect**

Fabien B. L. Cougnon,**[†] Kenji Caprice,[†] Marion Pupier,[†] Antonio Bauzá,[‡] and Antonio Frontera

Supporting Information

ABSTRACT: Conventional approaches to the synthesis of molecular knots and links mostly rely on metal templation. We present here an alternative strategy that uses the hydrophobic effect to drive the formation of complex interlocked structures in water. We designed an aqueous dynamic combinatorial system that can generate knots and links. In this system, the selfassembly of a topologically complex macrocycle is thermodynamically favored only if an optimum packing of all its components minimizes the hydrophobic surface area in contact with water. Therefore, the size, geometry, and rigidity of the initial building blocks can be exploited to control the formation of a specific topology. We illustrate the validity of this concept with the syntheses of a Hopf link, a Solomon link, and a trefoil



knot. This latter molecule, whose self-assembly is templated by halides, binds iodide with high affinity in water. Overall, this work brings a fresh perspective on the synthesis of topologically complex molecules: Solvophobic effects can be intentionally harnessed to direct the efficient and selective self-assembly of knots and links.

INTRODUCTION

Nearly 30 years after the synthesis of the first molecular trefoil knot, topologically complex molecules remain extremely difficult to produce and their properties are nearly unexplored.² In traditional synthetic approaches, ligands are pre-organized using metal coordination and linked together to generate molecular knots and links. This approach, originally devised by Sauvage,³ who notably synthesized a trefoil knot¹ and a Solomon link⁴ from linear helicates, has been more recently revisited by Leigh.^{2b,5-7} The Leigh group considerably expanded the complexity of available interlocked architectures by replacing linear helicates with circular helicates. Their most impressive example is probably the recent synthesis of a 819 knot with eight crossings.^{7,8} Surprisingly, supramolecular interactions other than metal coordination have rarely been employed to promote the synthesis of knots. 9-12 Using donor-acceptor π - π interactions to build structures more complex than singly interlocked catenanes has proved challenging. 2,8h Recent studies by Sanders et al. demonstrated that macrocycles could adopt nontrivial topologies in water to minimize solvent exposed hydrophobic surfaces. 11,12 The idea that the hydrophobic effect, 11-15 and perhaps more generally solvophobic effects, could provide an alternative driving force to promote the formation of knots and links in the absence of metals is extremely appealing. However, translating these observations into a reliable synthetic strategy represents a critical step that has not been overcome until today.

We present now a strategy that uses the hydrophobic effect to direct the synthesis of knots and links. We considered the virtual hydrazone-based dynamic combinatorial library 16-18 (Figure 1) engendered by dialdehyde A (blue cartoon) and dihydrazide H (transparent cartoon). Dialdehyde A is a hydrophobic building block constituted of two quinolinium-5carboxaldehyde units connected with a p-xylyl unit. Dihydrazide H is a fictive neutral hydrophobic building block that could be ideally stretched and bent to enable the closure of any macrocycle. Folding the quinolinium-based units (A) in a loop-like conformation around the neutral hydrophobic moiety of H represents the optimum way to decrease the number of hydrophobic surfaces exposed to the environment. The permanent positive charges of the quinolinium units remains on the outer surface, while the neutral moiety H and a large part of the aromatic surfaces of A are sheltered from water.

This motif was simply multiplied with an *n*-fold rotation axis $(C_n \text{ or } S_n)$ to construct macrocycles with minimum surface area exposed to water. Each time, we obtained a unique architecture. These architectures consistently alternated blue and transparent components and were characterized by a topological complexity of n crossings (Figure 1). A C_2 axis generated a Hopf link or singly interlocked [2]catenane (two crossings); a C_3 axis generated a trefoil knot (three crossings); a C_4 axis

Received: May 18, 2018 Published: August 28, 2018

Department of Organic Chemistry, University of Geneva, 30 Quai Ernest-Ansermet, 1211 Geneva 4, Switzerland

[‡]Department de Química, Universitat de les Illes Balears, Carretera de Valldemossa km 7.5, 07122 Palma de Mallorca, Baleares, Spain

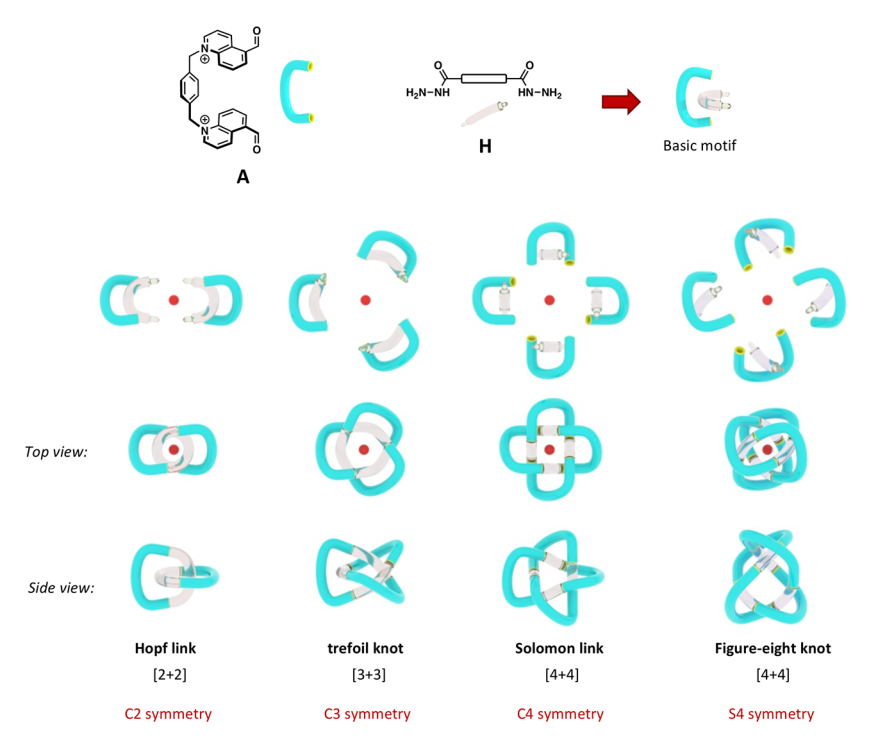


Figure 1. A virtual dynamic combinatorial library of knots and links generated from dialdehyde A (blue cartoon) and a fictive dihydrazide **H** (transparent cartoon). All these structures were constructed from a basic motif (top right) multiplied n times using an axis of symmetry C_n or S_n (represented by the red dot).

generated a Solomon link or doubly interlocked [2]catenane (four crossings); a S₄ axis generated a figure-eight knot (four crossings), etc. The list presented here, intentionally limited to the simplest topologies tabulated by mathematicians, 19 is nonexhaustive. Many other topologies could be similarly constructed through the same process of multiplication. Building blocks A and H could therefore ideally produce a complex library of knots and links. Macrocycles with trivial topologies may also form, but their formation should not be thermodynamically favored because their hydrophobic surfaces would remain exposed to water. Even from the simplified cartoon representation showed in Figure 1, it is noticeable that building block A (blue cartoon) can only generate all these topologies if H is indefinitely stretchable and bendable. Indeed, each topology enforces specific geometrical constraints on their backbone. This consideration was important as it suggested that the geometry and the flexibility of building block H could be used to bias the outcome of this virtual library in favor of a given

Here, we demonstrate that the choice of the dihydrazide (H1-3) is indeed critical and allows for the selective amplification of three topologies from the virtual pool described above: a Hopf link, a Solomon link, and a trefoil knot. The syntheses described here are the result of a rapid screening of readily available dihydrazides. In the following sections, we describe these syntheses as three independent stories. In each case, we also investigated the role of the quinolinium counterion (X⁻) on the outcome of the libraries. We first prepared analytical-scale hydrazone-based dynamic combinatorial libraries following a protocol optimized by Sessler¹⁵ and Li.²⁰ Equimolar amounts of dialdehyde A·2X (2.5 mM) and dihydrazide H1-3 (2.5 mM) were dissolved in D_2O (700 μ L, 0.01% TFA). The libraries were stirred overnight at 70 °C. The structures formed were all purified by semipreparative HPLC. During the process of purification, the counterion X was

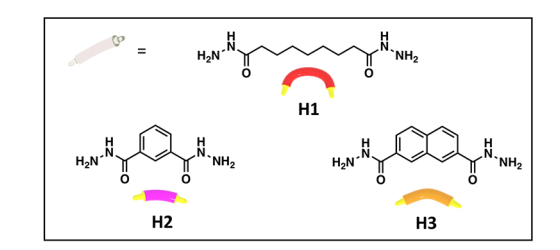
replaced by the trifluoroacetate anion present in the HPLC eluent. All the products were thus isolated as trifluoroacetate

We identified knots and links using ¹H NMR and ion-spray mass spectrometry (ESI-MS). The interlocked structures represented in Figure 1 feature n equivalent arms, each comprised an outer quinolinium-based loop (originating from dialdehyde A) surrounding an inner thread (originating from dihydrazide H). In all these structures, the moiety H is buried inside and inevitably experiences a symptomatic NMR shielding.

ESI-MS provided additional structural information and notably allowed for the characterization of the type of topology formed: A Hopf link is a [2 + 2] species and fragments into two [1 + 1] species; a trefoil knot is a [3 + 3] species and fragments as a single macrocycle; a Solomon link is a [4 + 4] species and fragments into two [2 + 2] species; a figure-eight knot is a [4 + 4] species and fragments as a single macrocycle, etc. If the identification of the topologies formed becomes more difficult as the number of crossing increases, this analytical method allows for the differentiation of the simplest knots and links shown in Figure 1.

Finally, theoretical calculations of the knots and links were carried out using the DFT-D3 methodology, providing useful information regarding the adequate conformation of each building block within the interlocked architectures. The optimized geometries compared well with the NMR data and provided further evidence of the structural viability of the knots and links synthesized.

A Hopf Link, or Singly Interlocked [2] Catenane. Highperformance liquid chromatography (HPLC, Figure 2a) revealed that A·2X and dihydrazide H1 generated a rather simple library, mostly dominated by one product, $1 (\sim 70\%)$. This outcome was independent of the choice of the counterion X^- (Figure S51). ESI-MS analysis showed that 1 was a [2 + 2]species. Three major peaks at mass-to-charge ratio m/z 299.15,



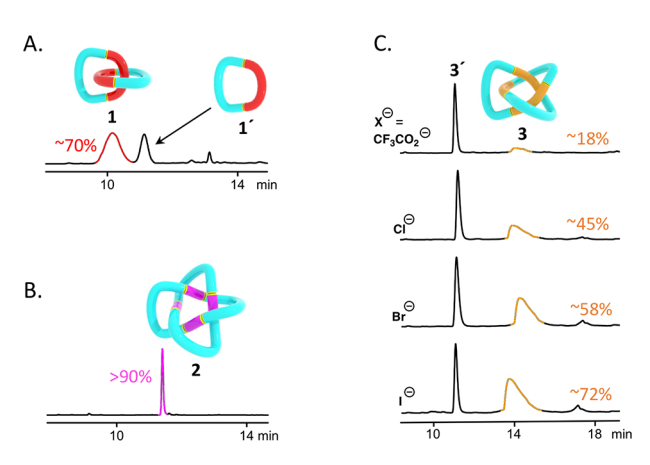


Figure 2. HPLC traces of the libraries generated from dialdehyde A. 2X (2.5 mM) and dihydrazide (a) H1, (b) H2, and (c) H3 (2.5 mM). The yields were evaluated from the integration of the peak areas using catechol as an internal standard. The HPLC traces of the libraries prepared from A·2X and H1, or from A·2X and H2, were identical for any of the counterions X^- tested (Figure S51).

398.54, and 597.29, corresponded to $[1]^{4+}$, $[1 - H]^{3+}$, and $[1-2H]^{2+}$, respectively (Figure S15). At a collision voltage of 45 V, dissociation of 1 yielded a fragmentation pattern characteristic of a [2] catenane composed of two interlocked [1 + 1]macrocycles (Figure S17). The [2 + 2] species 1 is relatively simple and cannot be interlocked more than once, implying that 1 was a singly interlocked [2]catenane, or Hopf link.

The Hopf link 1 was isolated by HPLC and further characterized by ¹H NMR in D₂O. The spectrum of 1·4CF₃CO₂ at 298 K (Figure 3a) confirmed that it was composed of two identical arms, each constituted of a quinolinium-based loop (A) threaded by the aliphatic chain (H1). Threading of the aliphatic chain was clearly manifested by a significant upfield shift of the aliphatic protons k, l, and m (below 0 ppm) compared to the same protons in the parent building block H1 (~1.16-1.78 ppm). Moreover, relatively intense nuclear Overhauser effect (NOE) cross-peaks between the aliphatic protons and the surrounding quinolinium and xylyl protons supported the proposed structure (Figure S10). In spite of its interlocked nature, 1 remained a flexible structure. The ability of the hydrazone bond to rotate freely was notably highlighted by the presence of NOE correlations between the hydrazone proton a and both protons b and g of the neighboring quinolinium (Figure S9). Furthermore, the presence of several minor conformations in dynamic exchange was noticeable at 298 K. Their proportion considerably increased at lower temperatures (below 298 K, Figure S7).

The minimum energy structure of the Hopf link is represented in Figure 3c. The H atoms of the flexible aliphatic chain were located between the quinolinium π -systems, in agreement with the upfield shift observed by NMR. The analysis of bond lengths and angles indicated that this link did not present any

strained functional group, bond or ring, thus explaining its dominant formation (\sim 70%).

The same library also contained a small amount of the [1 + 1] macrocycle 1' (~25%, Figure 2a). We isolated 1'-2CF₃CO₂ to compare its NMR features to that of the Hopf link 1.4CF3CO2. Macrocycle 1' can only be topologically trivial and did not feature any major change of chemical environment compared to the original building blocks (Figure S6). The only noteworthy exception was that of the aldehyde proton a (10.42 ppm in A) transformed during the reaction into a hydrazone proton (8.65 ppm in 1').

The self-assembly of a Hopf link (1), driven by the hydrophobicity of the aliphatic moiety, is in full agreement with findings reported in other studies. ^{14,20} We also explored the effect of the length of the aliphatic chains (Figure S57). The formation of the Hopf link was always favored if the length of the aliphatic chain was superior or equal to $(-CH_2-)_6$. In all these cases, the simplest nontrivial topology is formed because the aliphatic chain is highly flexible. Introducing more rigidity in the backbone of the dihydrazide building block should prevent the formation of a Hopf link, thereby opening up the possibility to build other more complex topologies. It is precisely what was observed in the two following libraries, obtained from the rigid isophthalic (H2) and 2,7-naphthalene (H3) building

A Solomon Link, or Doubly Interlocked [2] Catenane. The HPLC trace in Figure 2b showed that reaction between A·2X and the isophthalic dihydrazide H2 almost exclusively generated a single product, 2 (>90%). Here again, this outcome was independent of the counterion X used (Figure S51). To our surprise, ESI-MS indicated that 2 was a [4 + 4] species $(m/z [2-4H]^{4+} = 575.18, [2-5H]^{3+} = 766.91, [2-6H]^{2+} =$ 1150.36, Figure S30). The exclusive self-assembly of such a large macrocycle was remarkable and immediately caught our attention. Collision-induced dissociation of 2 produced a fragmentation pattern corresponding to a [2]catenane composed of two interlocked [2 + 2] macrocycles (Figure S31). This fragmentation pattern immediately ruled out the possibility that 2 could be a trivial or a knotted macrocycle, such as a figureeight knot. On the other hand, two [2 + 2] macrocycles may be interlocked more than once, raising our hope that 2 would exhibit a topology more complex than that of a Hopf link.

The ¹H NMR spectrum of the isolated [4 + 4] species 2.8CF₃CO₂ in D₂O was significantly complex (Figure 4a), with aromatic protons spanning an astonishingly wide range of chemical shifts from 10.91 to 3.88 ppm. The spectrum displayed sharp signals corresponding to a molecule composed of four identical arms, each constituted of a quinolinium-based loop (A) threaded by an isophthalic moiety (H2). The unexpected complexity of the spectrum arose from the inequivalence of every proton within an individual arm. The most significant upfield shifts, compared to the parent building blocks, were observed for the isophthalic protons k (7.94 ppm in H2 to 3.88 ppm in 2) and 1 (7.66 ppm in H2 to 6.04 ppm in 2). These shifts not only indicated that the isophtahlic moiety was stacked between the quinolinium units but also that protons k and I were pointing directly toward the perpendicular xylyl unit. Proton j, located on the opposite side of the isophathlic unit, was therefore oriented toward the central cavity of the molecule. As a consequence, it did not experience any strong shielding effect from nearby aromatic units (8.07 ppm in H2 versus 7.98 ppm in 2).

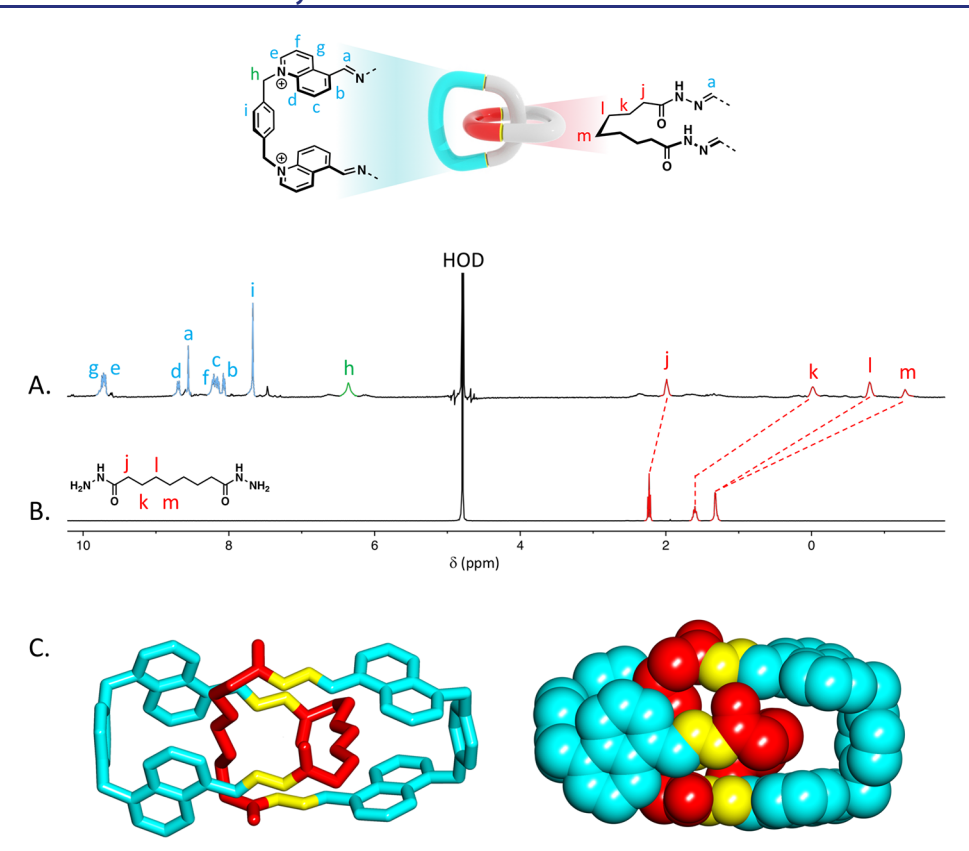


Figure 3. Comparison between the ¹H NMR spectra (500 MHz, 298 K, D₂O) of (a) the Hopf link 1·4CF₃CO₂ and (b) the parent dihydrazide building block H1. (c) BP86-D3/def2-TZVP optimized geometry of Hopf link 1 in sticks (left) and space filling (right). H atoms were omitted for clarity. The hydrazone bonds were represented in yellow, moiety A in blue, and moiety H1 in red.

Each arm of the structure possessed two hydrazone bonds, with one on each side of the isophthalic moiety. NOE correlations obtained in a 95:5 H₂O/D₂O mixture (Figure S25) disclosed that these two hydrazone bonds adopted different conformations, with one NH pointing toward the interior (observed correlations: $\mathbf{i} \leftrightarrow \mathbf{NH} \leftrightarrow \mathbf{a} \leftrightarrow \mathbf{b}$) and another one pointing toward the exterior (observed correlations: $k' \leftrightarrow NH'$ \leftrightarrow a' \leftrightarrow g') of the structure. To conclude, the full analysis of this spectrum highlighted that 2 was a rigid, twisted molecule locked into a well-defined conformation. Importantly, two pairs of diastereotopic protons (h and h') suggested that the topology of 2 induced a chiral environment. The only topology consistent with such an NMR spectrum, with the mass of a [4 + 4] species and with the MS/MS fragmentation pattern observed, is the topology of a Solomon link, or doubly interlocked [2]catenane.

At higher temperatures, exchange cross-peaks appeared between pairs of inequivalent protons ($\mathbf{a}\leftrightarrow\mathbf{a}',\mathbf{b}\leftrightarrow\mathbf{b}',$ etc.), corresponding to a global inversion of the conformation of all the eight hydrazone bonds ($\mathbf{NH}\leftrightarrow\mathbf{NH}'$) of the molecule. The activation parameters were calculated from the cross-peaks intensity at variable temperatures (Figures S22 and S23). An unfavorable enthalpy of activation ($\Delta H^{\ddagger}=+115\ \mathrm{kJ\cdot mol^{-1}}$) and a favorable entropy of activation ($\Delta S^{\ddagger}=+106\ \mathrm{J\cdot K^{-1}\cdot mol^{-1}}$) contributed to a rather large energy barrier ($\Delta G^{\ddagger}=+838\ \mathrm{kJ\cdot mol^{-1}}$) at 298 K), reflecting the penalty associated with the reorganization of the entire structure.

The C_4 -symmetric Solomon link was easy to model using an antiparallel conformation of the quinolinium moieties in each arm and an opposite conformation of the two hydrazone bonds located at both sides of the isophthalic moiety (see Figure 4c,

pink fragments). The minimum energy structure agrees well with the NOE correlations (Figures S24 and S25), providing further support to the formation of the Solomon link. In addition, the DFT-D3 study on this system strongly supported the idea that the formation of a figure-eight knot from building blocks A and H2 was not possible: All attempts to model the figure-eight knot topology were unsuccessful due to its highly strained geometry.

The near-quantitative self-assembly of Solomon link 2 demonstrated the importance of introducing rigidity in the design of the dihydrazide building block to favor the formation of complex topologies. The yield of the synthesis was particularly impressive, presumably because the geometry of each unit allowed an optimum packing of all the hydrophobic aromatic surfaces. Indeed, when the same reaction was performed with the closely related terephthalic dihydrazide, we only observed the formation of a complex mixture of products with undecipherable NMR features (Figure S56). The angle between the hydrazide bonds thus seemed to be of crucial importance. Therefore, when we designed building block H3, we maintained a similar rigidity and a similar angle between the hydrazide bonds, and we chose to increase the π surface.

A Trefoil Knot. The 2,7-naphthalene-based dihydrazide building block H3 (Figure 2c) also generated a relatively simple library composed of two main species, a [3 + 3] species $(3, m/z [3 - 3H]^{3+} = 625.23, [3 - 4H]^{2+} = 937.84$, Figure S45) and a [4 + 4] species $(3', m/z [3'-2H]^{6+} = 417.14, [3' - 3H]^{5+} = 500.57, [3' - 4H]^{4+} = 625.20$, Figure S46). The formation of two such large macrocycles was already intriguing. More importantly, the HPLC traces depicted in Figure 2c showed that the outcome of the library was highly dependent on the

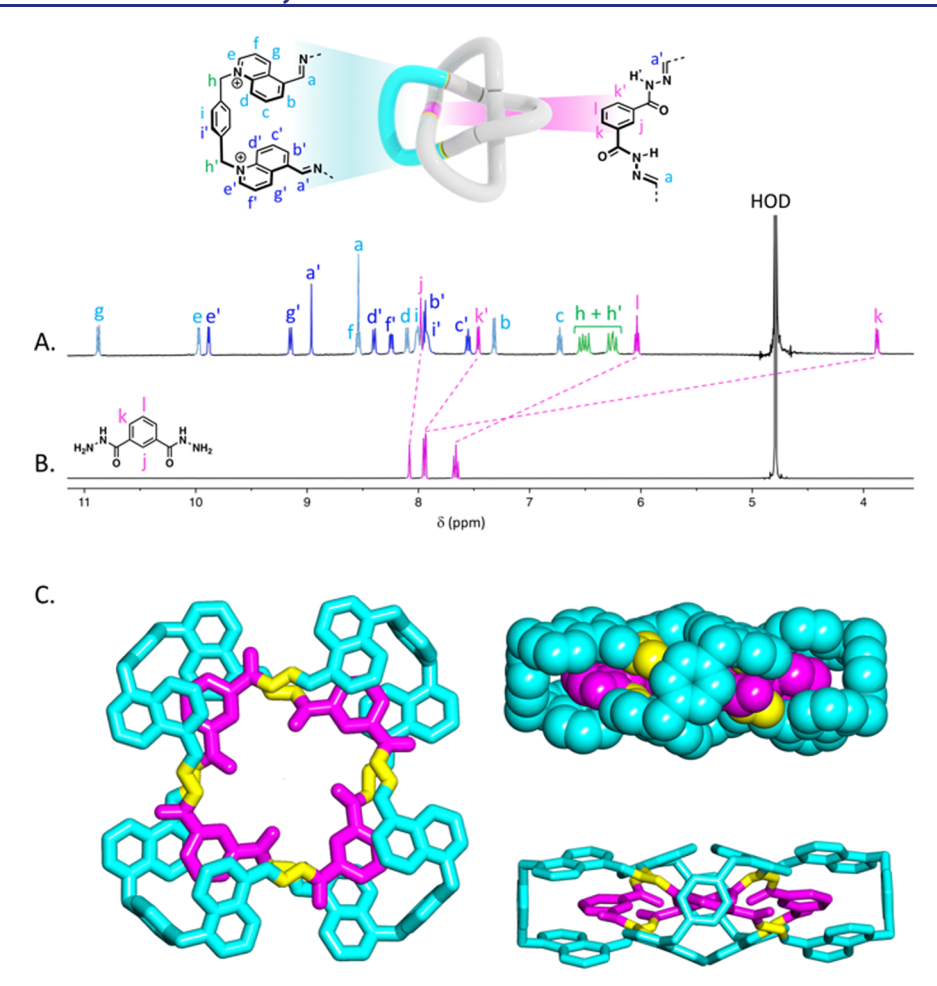


Figure 4. Comparison between the ¹H NMR spectra (500 MHz, 298 K, D₂O) of (a) the Solomon link 2·8CF₃CO₂ and (b) the parent dihydrazide building block H2. (c) Several views of the BP86-D3/def2-TZVP optimized geometry of Solomon link 2. H atoms were omitted for clarity. The hydrazone bonds were represented in yellow, moiety A in blue, and moiety H2 in pink.

choice of the counterion X^- . Only trace amounts of 3 were found in the absence of halides ($X^- = CF_3CO_2^-$). In the presence of halides ($X^- = CI^-$, Br^- or I^-), 3 was formed in non-negligible quantities. The yield of 3 increased regularly with the size of the anion, from ~45% for the smallest halide used (CI^-) to ~72% for the largest one (I^-). This amplification phenomenon²³ strongly suggested that 3 was binding halides in a size-dependent manner. Selective anion recognition is challenging in pure water,²⁴ so we focused our attention on the characterization of 3.

After HPLC purification, the [3 + 3] macrocycle 3.6CF₃CO₂ displayed broad, featureless, uninterpretable ¹H MNR signals in D₂O (Figure 5a), indicating its ability to adopt many conformations in slow exchange. We were delighted to observe a progressive signal sharpening upon addition of either NaCl, NaBr, or NaI (Figure S34). Figure 5b shows, as a typical example, the spectrum of 3.6CF3CO2 after addition of ca. 10 equiv of NaBr. Minor conformations remained visible in the spectrum baseline after addition of NaBr (Figures S34 and S39). However, the spectrum of the bromide-bound macrocycle mainly showed a single conformation that echoed a highly symmetrical structure, consistent with a molecule composed of three identical arms, each constituted of a quinolinium-based loop (A) threaded by the naphthalene moiety (H3). Compared to the parent building block H3, the symptomatic upfield shift of the naphthalene protons I (7.91 to 4.14 ppm) and k (8.10 to

6.98 ppm) suggested that (1) each naphthalene moiety was stacked between two quinoliniums and (2) protons I and k were pointing toward the xylyl unit.

Such a spectrum and the mass of a [3+3] species were indicative of a trefoil knot topology. In agreement with this interpretation, the presence of diastereotopic protons (h1 and h2) reflected a topologically chiral environment. NOE correlations (b \leftrightarrow a \leftrightarrow NH \leftrightarrow j, Figure S37) in a 95:5 H₂O/D₂O mixture revealed that all the six hydrazone bonds of the bromide-bond macrocycle adopted an identical conformation. Protons NH and j were both oriented toward the center of the molecule, and a total of six NH hydrazone pointing toward the central cavity provided an ideal binding site for halides. The presence of bromide at the center of the molecule was further confirmed by a downfield shift of the nearby proton j (from 8.14 in H3 to 9.32 ppm in 3).

We also succeeded in constructing and optimizing the trefoil knot using DFT-D3 calculations. The optimized geometry in water showed that the central cavity should be able to incorporate two spherical anions (Cl $^-$, Br $^-$, or I $^-$) since six NH groups were pointing to the main symmetry axis in two different layers, thus generating a ditopic cavity (Figure S58). In Figure 5d, we show the optimized geometry of the trefoil knot interacting with two bromide anions in water. The minimum energy structure presents C_3 symmetry where each Br atom interacts with three NH and three CH groups, thus

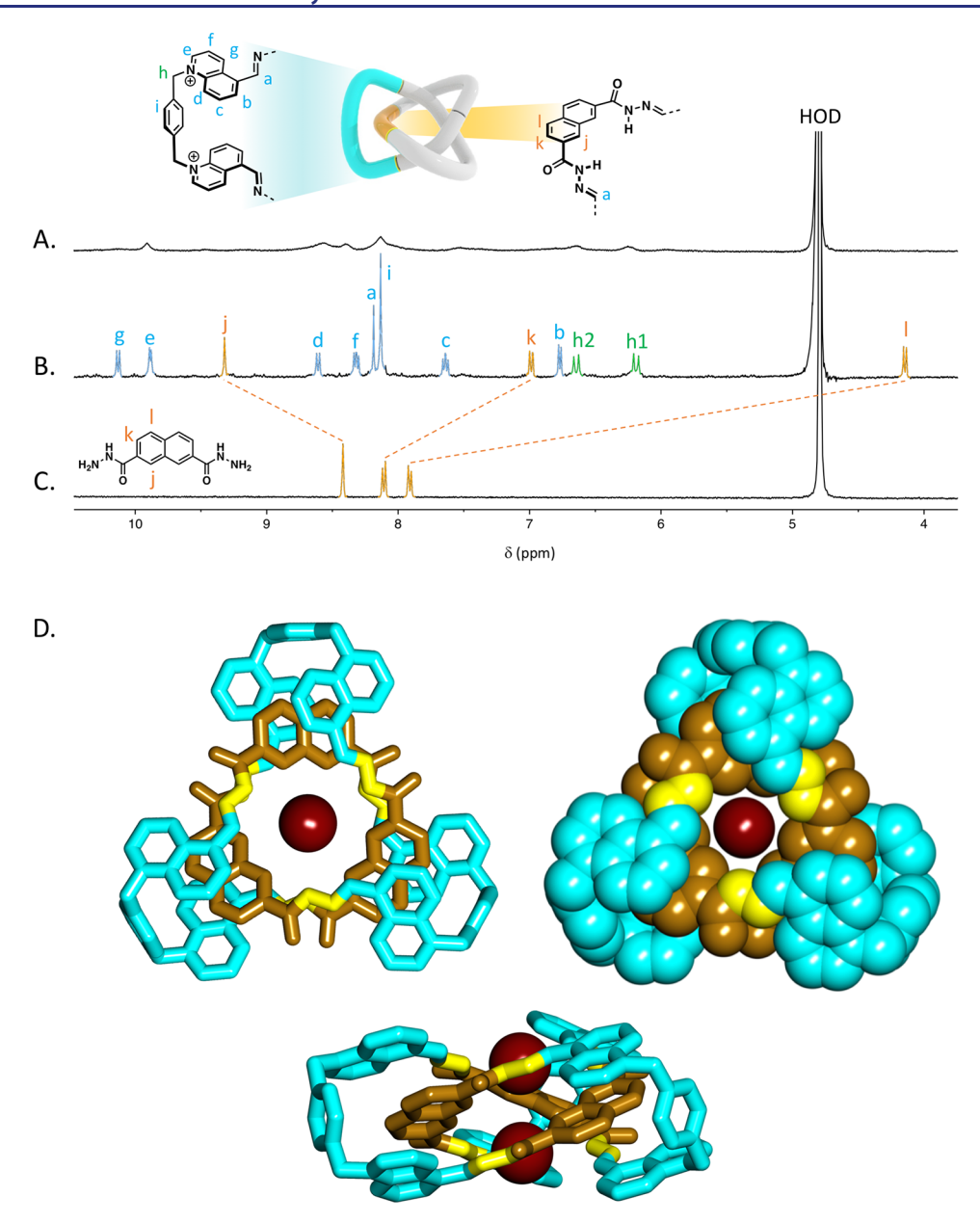


Figure 5. Comparison between the ¹H NMR spectra (500 MHz, 298 K, D₂O) of (a) the trefoil knot 3·6CF₃CO₂, (b) the trefoil knot 3·6CF₃CO₂ in the presence of ca. 10 equiv of NaBr, and (c) the parent dihydrazide building block H3. (d) Several views (sticks and CPK) of the BP86-D3/def2-TZVP optimized geometry of the trefoil knot 3 complexed to two bromide anions (3 could also accommodate two iodide ions). H atoms were omitted for clarity. The hydrazone bonds were represented in yellow, moiety A in blue, and moiety H3 in gold.

establishing six hydrogen bonds (Figure S58B). We concluded that the amplification originally observed in the libraries (Figure 2c) could be explained by the selective binding of halides to the central cavity of the [3 + 3] trefoil knot 3·6CF₃CO₂ rather than to the [4 + 4] macrocycle 3′·8CF₃CO₂. Indeed, no interaction between the [4 + 4] macrocycle 3′·8CF₃CO₂ and halides could be evidenced by NMR (Figure S35), microcalorimetry (Figure S50), and ESI-MS (Figure S47). Unfortunately, 3′·8CF₃CO₂ displayed broad NMR signals in D₂O, even at high temperatures and after addition of NaBr (Figure S35). Consequently, the structural basis underlying its lack of interaction with halides remained unknown.

We explored the interaction between the [3 + 3] macrocycle $3.6\text{CF}_3\text{CO}_2$ and each halide by microcalorimetry (Figure S49). As expected, the strongest binding was observed with iodide (NaI). The data confirmed that 2 equiv of iodide could bind

with high affinity ($K = 1.6 \times 10^4 \ \mathrm{M}^{-1}$). Binding was driven both by enthalpy ($\Delta H = -20.2 \ \mathrm{kJ \cdot mol^{-1}}$) and by entropy ($\Delta S = +12.8 \ \mathrm{J \cdot K^{-1} \cdot mol^{-1}}$). Early saturation during the titration with NaBr indicated that binding with bromide was about an order of magnitude lower, but the binding constant could not be measured. Nevertheless, the stoichiometry of both the iodide and the bromide complexes were confirmed by ESI-MS, as both the unbound ($[3 - 2H]^{4+}$) and bound ($[3 + 2X]^{4+}$) species were identified (Figure S47) in the MS spectra of the crude libraries. We compared theoretically the affinity of 3 for bromide and iodide by evaluating the following substitution reaction:

$$3 \cdot 2Br^{-} + 2[I(H_2O)_6]^{-} \rightarrow 3 \cdot 2I^{-} + 2[Br(H_2O)_6]^{-}$$
 (1)

We used explicit water molecules in the first coordination sphere and a dielectric continuum model (COSMO) to account for solvent effects. This procedure was more convenient than the direct comparison of interaction energies because the energy of the free knot at room temperature was not needed. The reaction energy of the substitution of bromide by iodide (eq 1 and Figure S59) at the BP86-D3/def2-TZVP level of theory was energetically favorable ($\Delta G = -10.03 \text{ kJ} \cdot \text{mol}^{-1}$), which was good agreement with the experimental data that suggested that binding of bromide was an order of magnitude lower compared to iodide. Binding with chloride, presumably even weaker, could not be measured by microcalorimetry either. The adduct $[3 + 2Cl]^{4+}$ also remained elusive in ESI-MS. Overall, the affinity of 3.6CF₃CO₂ with halides appeared to be weaker than we had expected from the magnitude of the amplifications observed during the synthesis. It is noteworthy to mention that the CF₃CO₂⁻ anion is likely to interact with the NHs of the trefoil knot and probably competes with the binding of halides during the microcalorimetric titrations performed on the isolated trifluoroacetate salt 3.6CF3CO2. In contrast, only a catalytic amount of trifluoroacetic acid was present during the syntheses carried out using the halide salts A.2X.

The self-assembly of trefoil knot 3 is driven by the hydrophobicity of the naphthalene moiety and is templated by halides, which presumably direct all the hydrazone bonds in the conformation required to close the structure. Several knots and links binding halides in their central cavities have already been reported. 5,27-29 Here, this last example highlights that a complex interplay of subtle interactions can participate in the selection of a specific topology. The broad NMR features of 3.6CF₃CO₂ in D₂O in the absence of halides (Figure 5a) remained puzzling. To complete this study, we performed additional experiments to ascertain the knotted topology of 3.6CF₃CO₂. The ability of a molecule to adopt many conformations in slow exchange is highly dependent on the solvent used. On the other hand, a knot cannot unfold once it has been closed and maintains its topology independently of the solvent used. Illustrating these two statements, we observed that the ¹H NMR signals of 3.6CF₃CO₂ in CD₃CN were sharp and retained all the symptomatic features characteristic of a trefoil knot (e.g., diasteretopic protons and significantly upfield-shifted naphthalene protons, Figure S43). Furthermore, splitting of the signals upon addition of the anionic chiral shift reagent (R)-2-phenyl-propioniate corroborated that 3 was produced as a racemic mixture of two enantiomers, the rightand left-handed knots (Figure S44).

With this trefoil knot, we complete a first catalogue of several structures with complex topologies. The hydrodynamic radii $R_{\rm H}$, evaluated from the NMR diffusion coefficients (Figures S11, S26, and S38), mirrored the difference in size between all these species: 0.66 nm for the [1+1] species 1'; 0.72 nm for the [2+2] species 1; 0.87 nm for the [3+3] species 3; and 1.06 nm for the [4+4] species 2. These values are in reasonable agreement with the theoretical values (0.57 nm for 1', 0.64 nm for 1, 0.92 nm for 3, and 1.12 nm for 2).

■ CONCLUSIONS

To conclude, we proposed an original strategy to synthesize molecules with complex topologies, and we illustrated our approach with the synthesis of three structures: a Hopf link (1), a Solomon link (2), and a trefoil knot (3). We are working on obtaining crystals suitable for diffraction to prove these topologies unambiguously. Identifying topologies before obtaining an X-ray crystal structure is a challenging intellectual

puzzle. We applied a solution-based analytic method to characterize the type of topology formed, and the results of our interpretation were all confronted with success to DFT calculations. In some cases (3 and 3'), the lack of 1H NMR signals in D_2O increased the difficulty to assign the topology of the isolated macrocycles. If crystal structures ultimately confirm the topology of all three molecules 1-3, this work will probably represent the simplest strategy to date to access molecular knots and links. Our approach is simple, cheap, particularly high-yielding, and requires minimum effort in terms of synthesis and purification.

The formation of these interlocked architectures was relatively fast (<3 h, Figure S55) and mostly driven by the hydrophobic effect. Indeed, the yield of the three macrocycles 1-3 decreased when the libraries were prepared in water/DMSO mixtures (Figure S52). However, the structures survived a relatively large ratio of DMSO (>20% of DMSO in the case of 2 and 3), suggesting that several supramolecular interactions such as intramolecular hydrogen bonds, hydrogen halide bonds, and $\pi-\pi$ interactions also intervene in the process of self-assembly.

The interlocked structures 1-3 are stable in the aqueous medium for several weeks. The hydrazone bond is reversible, but each intertwined molecule represents a kinetic trap from which it is difficult to escape (Figure S53). In contrast, non-interlocked macrocycles such as the trivial [1+1] macrocycle $\mathbf{1}'$ continue to evolve over time. The NMR spectrum of the isolated sample of $\mathbf{1}' \cdot \mathbf{4}\mathbf{C}\mathbf{F}_3\mathbf{C}\mathbf{O}_2$ left for two months in the fridge (278 K) in $\mathbf{D}_2\mathbf{O}$ in neutral conditions showed a slow reorganization into the more stable Hopf link $\mathbf{1}$ (Figure S54).

From a more fundamental perspective, the hydrophobicity, the size, and the geometry of the building blocks are certainly determining factors in the process of selection and amplification of a specific topology from a virtual dynamic pool of knots and links. The exact nature of the relationship between the type of dihydrazide building block employed and the topology naturally selected is not yet understood. It is currently impossible to predict the formation of a knot or a link in our system. Due to the simplicity of implementation, the system presented here should nevertheless allow us to understand better how the hydrophobic effect can be exploited to construct specific topologies. The hydrophobicity of the building blocks is undoubtedly the main feature that drives the formation of metal-free molecular knots and links in water. Therefore, we expect that our strategy will not be limited to quinolinium-based building blocks and may be generalizable to other hydrophobic chemical structures. A synergetic combination of the hydrophobic effect and donor-acceptor π - π interactions or metal templation may prove particularly powerful in the future.

ASSOCIATED CONTENT

S Supporting Information

The Supporting Information is available free of charge on the ACS Publications website at DOI: 10.1021/jacs.8b05220.

The synthesis and characterization (¹H and ¹³C NMR, HR-MS, and MS/MS) of the building blocks and of the interlocked structures **1**–**3** are available as well as computational methods and Cartesian coordinates of all optimized complexes. We also provide additional figures with the optimized structures and details on the binding energy calculations of the halide complexes (PDF)

AUTHOR INFORMATION

Corresponding Author

*fabien.cougnon@unige.ch

ORCID ®

Fabien B. L. Cougnon: 0000-0003-4487-8707 Antonio Bauzá: 0000-0002-5793-781X

Antonio Frontera: 0000-0001-7840-2139

Notes

The authors declare no competing financial interest.

ACKNOWLEDGMENTS

This work is dedicated to Prof. Jeremy K. M. Sanders. We would like to take the opportunity to thank him for his kind support and for allowing us to use his LC-MS. The Swiss National Science Foundation (PZ00P2 161270), the Department of Organic Chemistry at the University of Geneva, and the MINECO/AEI of Spain (projects CTQ2014-57393-C2-1-P and CTQ2017-85821-R FEDER funds) are gratefully acknowledged for financial support. We thank Dr. Ana Belenguer for help with the LC-MS. We also thank Dr. Daniel Palomino and Irina Dorin (Malvern Panalytical Ltd) for help with ITC data processing. Finally, we acknowledge Emmanuel Varesio, Harry Théraulaz, and Eliane Sandmeier at the Mass Spectrometry Core Facility of the University of Geneva for performing thorough HR-MS characterizations.

REFERENCES

- (1) Dietrich-Buchecker, C. O.; Sauvage, J.-P. Angew. Chem., Int. Ed. Engl. 1989, 28, 189.
- (2) (a) Forgan, R. S.; Sauvage, J.-P.; Stoddart, J. F. Chem. Rev. 2011, 111, 5434. (b) Ayme, J.-F.; Beves, J. E.; Campbell, C. J.; Leigh, D. A. Chem. Soc. Rev. 2013, 42, 1700. (c) Fielden, S. D. P.; Leigh, D. A.; Woltering, S. L. Angew. Chem., Int. Ed. 2017, 56, 11166.
- (3) Sauvage, J.-P. Acc. Chem. Res. 1990, 23, 319.
- (4) Nierengarten, J.-F.; Dietrich-Buchecker, C. O.; Sauvage, J.-P. J. Am. Chem. Soc. 1994, 116, 375.
- (5) Ayme, J.-F.; Beves, J. E.; Leigh, D. A.; McBurney, R. T.; Rissanen, K.; Schultz, D. Nat. Chem. 2012, 4, 15.
- (6) Leigh, D. A.; Pritchard, R. G.; Stephens, A. J. Nat. Chem. 2014, 6,
- (7) Danon, J. J.; Krüger, A.; Leigh, D. A.; Lemonnier, J. F.; Stephens, A. J.; Vitorica-Yrezabal, I. J.; Woltering, S. L. Science 2017, 355, 159.
- (8) For other examples of successful syntheses of knots and links, see: (a) Chichak, K. S.; Cantrill, S. J.; Pease, A. R.; Chiu, S.-H.; Cave, G. W. V.; Atwood, J. L.; Stoddart, J. F. Science 2004, 304, 1308. (b) Prakasam, T.; Lusi, M.; Elhabiri, M.; Platas-Iglesias, C.; Olsen, J.-C.; Asfari, Z.; Cianférani-Sanglier, S.; Debaene, F.; Charbonnière, L. J.; Trabolsi, A. Angew. Chem., Int. Ed. 2013, 52, 9956. (c) Carina, R. F.; Dietrich-Buchecker, C.; Sauvage, J.-P. J. Am. Chem. Soc. 1996, 118, 9110. (d) Sawada, T.; Yamagami, M.; Ohara, K.; Yamaguchi, K.; Fujita, M. Angew. Chem., Int. Ed. 2016, 55, 4519. (e) Guo, J.; Mayers, P. C.; Breault, G. A.; Hunter, C. A. Nat. Chem. 2010, 2, 218. (f) Wood, C. S.; Ronson, T. K.; Belenguer, A. M.; Holstein, J. J.; Nitschke, J. R. Nat. Chem. 2015, 7, 354. (g) Liu, Y.; Ma, Y.; Zhao, Y.; Sun, X.; Gándara, F.; Furukawa, H.; Liu, Z.; Zhu, H.; Zhu, C.; Suenaga, K.; Oleynikov, P.; Alshammari, A. S.; Zhang, X.; Terasaki, O.; Yaghi, O. M. Science 2016, 351, 365. (h) Peinador, C.; Blanco, V.; Quintela, J. M. J. Am. Chem. Soc. 2009, 131, 920.
- (9) Safarowsky, O.; Nieger, M.; Fröhlich, R.; Vögtle, F. Angew. Chem., Int. Ed. 2000, 39, 1616.
- (10) Elbaz, J.; Wang, Z.-G.; Wang, F.; Willner, I. Angew. Chem., Int. Ed. 2012, 51, 2349.
- (11) Ponnuswamy, N.; Cougnon, F. B. L.; Clough, J. M.; Pantoş, G. D.; Sanders, J. K. M. Science 2012, 338, 783.

- (12) Ponnuswamy, N.; Cougnon, F. B. L.; Pantoş, G. D.; Sanders, J. K. M. J. Am. Chem. Soc. 2014, 136, 8243.
- (13) Fujita, M.; Ibukuro, F.; Hagihara, H.; Ogura, K. Nature 1994,
- (14) Caprice, K.; Pupier, M.; Kruve, A.; Schalley, C. A.; Cougnon, F. B. L. Chem. Sci. 2018, 9, 1317.
- (15) Li, H.; Zhang, H.; Lammer, A. D.; Wang, M.; Li, X.; Lynch, V. M.; Sessler, J. L. Nat. Chem. 2015, 7, 1003.
- (16) For reviews on dynamic combinatorial chemistry, see: (a) Corbett, P. T.; Leclaire, J.; Vial, L.; West, K. R.; Wietor, J.-L.; Sanders, J. K. M.; Otto, S. Chem. Rev. 2006, 106, 3652. (b) Lehn, J.-M. Chem. Soc. Rev. 2007, 36, 151. (c) Li, J.; Nowak, P.; Otto, S. J. Am. Chem. Soc. 2013, 135, 9222. (d) Jin, Y.; Yu, C.; Denman, R. J.; Zhang, W. Chem. Soc. Rev. 2013, 42, 6634.
- (17) (a) Otto, S.; Furlan, R. L. E.; Sanders, J. K. M. J. Am. Chem. Soc. 2000, 122, 12063. (b) Otto, S.; Furlan, R. L. E.; Sanders, J. K. M. Science 2002, 297, 590. (c) Hasenknopf, B.; Lehn, J.-M.; Kneisel, B. O.; Baum, G.; Fenske, D. Angew. Chem., Int. Ed. Engl. 1996, 35, 1838. (d) Hasenknopf, B.; Lehn, J.-M.; Boumediene, N.; Dupont-Gervais, A.; Van Dorsselaer, A.; Kneisel, B. O.; Fenske, D. J. Am. Chem. Soc. 1997, 119, 10956. (e) Huc, I.; Lehn, J.-M. Proc. Natl. Acad. Sci. U. S. A. 1997, 94, 2106. (f) Carnall, J. M. A.; Waudby, C. A.; Belenguer, A. M.; Stuart, M. C. A.; Peyralans, J. J.-P.; Otto, S. Science 2010, 327, 1502. (g) Sadownik, J. W.; Mattia, E.; Nowak, P.; Otto, S. Nat. Chem. 2016, 8, 264. (h) Wang, Q.; Zhang, C.; Noll, B. C.; Long, H.; Jin, Y.; Zhang, W. Angew. Chem., Int. Ed. 2014, 53, 10663. (i) Wang, Q.; Yu, C.; Long, H.; Du, Y.; Jin, Y.; Zhang, W. Angew. Chem., Int. Ed. 2015, 54, 7550. (j) Brachvogel, R.; Maid, H.; von Delius, M. Int. J. Mol. Sci. 2015, 16, 20641. (k) Seoane, A.; Brea, R. J.; Fuertes, A.; Podolsky, K. A.; Devaraj, N. K. J. Am. Chem. Soc. 2018, 140, 8388.
- (18) For other uses of the acyl hydrazone bond in dynamic combinatorial chemistry, see: (a) Furlan, R. L. E.; Ng, Y.-F.; Otto, S.; Sanders, J. K. M. J. Am. Chem. Soc. 2001, 123, 8876. (b) Lam, R. T.; Belenguer, A.; Roberts, S. L.; Naumann, C.; Jarrosson, T.; Otto, S.; Sanders, J. K. M. Science 2005, 308, 667. (c) Beeren, S. R.; Pittelkow, M.; Sanders, J. K. M. Chem. Commun. 2011, 47, 7359. (d) Chung, M.-K.; White, P. S.; Lee, S. J.; Waters, M. L.; Gagné, M. R. J. Am. Chem. Soc. 2012, 134, 11415. (e) Chung, M.-K.; Lee, S. J.; Waters, M. L.; Gagné, M. R. J. Am. Chem. Soc. 2012, 134, 11430. (f) Cvrtila, I.; Fanlo-Virgós, H.; Schaeffer, G.; Santiago, G. M.; Otto, S. J. Am. Chem. Soc. 2017, 139, 12459. (g) Mondal, M.; Radeva, N.; Fanlo-Virfós, H.; Otto, S.; Klebe, G.; Hirsch, A. K. H. Angew. Chem., Int. Ed. 2016, 55,
- (19) Handbook of Knot Theory; Menasco, W., Thistlethwaite, M., Eds.; Elsevier Science: Amsterdam, 2005; p 209.
- (20) Wu, G.; Wang, C.-Y.; Jiao, T.; Zhu, H.; Huang, F.; Li, H. J. Am. Chem. Soc. 2018, 140, 5955.
- (21) Schill, G. Catenanes, Rotaxanes and Knots; Academic Press: New York, 1971.
- (22) Pons, M.; Millet, O. Prog. Nucl. Magn. Reson. Spectrosc. 2001, 38, 267.
- (23) For examples of anion recognition in dynamic combinatorial systems, see: (a) Otto, S.; Kubik, S. J. Am. Chem. Soc. 2003, 125, 7804. (b) Beeren, S. R.; Sanders, J. K. M. Chem. Sci. 2011, 2, 1560. (c) Beeren, S. R.; Sanders, J. K. M. J. Am. Chem. Soc. 2011, 133, 3804. (d) Katayev, E. A.; Pantoş, G. D.; Reshetova, M. D.; Khrustalev, V. N.; Lynch, V. M.; Ustynyuk, Y. A.; Sessler, J. L. Angew. Chem., Int. Ed. 2005, 44, 7386. (e) Riddell, I. A.; Smulders, M. M. J.; Clegg, J. K.; Hristova, Y. R.; Breiner, B.; Thoburn, J. D.; Nitschke, J. R. Nat. Chem. **2012**, *4*, 751.
- (24) (a) Busschaert, N.; Caltagirone, C.; Van Rossom, W.; Gale, P. A. Chem. Rev. 2015, 115, 8038. (b) Kubik, S. Chem. Soc. Rev. 2010, 39, 3648-3663. (c) Kim, Y.; Gabbaï, F. P. J. Am. Chem. Soc. 2009, 131, 3363.
- (25) When the library was prepared in DMSO from 10 mM of A. 2Br and 10 mM of H3 (Figure S33), we could identify by LC-MS another [3 + 3] macrocycle with a different retention time (20 min). This second [3 + 3] macrocycle is likely to be the topologically trivial macrocycle.

- (26) Due to the lack of feature of the unbound form of 3, it was not possible to determine the binding constants by NMR. Similarly, the UV—vis spectrum of 3 did not change upon addition of halides, and the binding constants could not be determined by UV titrations.
- (27) Bilbeisi, R. A.; Prakasam, T.; Lusi, M.; El-Khoury, R.; Platas-Iglesias, C.; Charbonnière, L. J.; Olsen, J.-C.; Elhabiri, M.; Trabolsi, A. *Chem. Sci.* **2016**, *7*, 2524.
- (28) Ayme, J.-F.; Beves, J. E.; Campbell, C. J.; Gil-Ramírez, G.; Leigh, D. A.; Stephens, A. J. *J. Am. Chem. Soc.* **2015**, *137*, 9812.
- (29) Other types of interlocked structures can bind anions: (a) Langton, M. J.; Robinson, S. W.; Marques, I.; Félix, V.; Beer, P. D. *Nat. Chem.* **2014**, *6*, 1039. (b) Caballero, A.; Zapata, F.; White, N. G.; Costa, P. J.; Félix, V.; Beer, P. D. *Angew. Chem., Int. Ed.* **2012**, *51*, 1876.